Enhancement of an automatic algorithm for deconvolution and quantification of three-dimensional microscopy images

Nathalie B. Vicente (nathalie.vicente@gmail.com)

Javier E. Diaz-Zamboni (javierdiaz@bioingenieria.edu.ar)

Javier F. Adur (jadur@bioingenieria.edu.ar)

María Fernanda Izaguirre (fizaguirre@bioingenieria.edu.ar)

Víctor H. Casco (vcasco@bioingenieria.edu.ar)

Microscopy Laboratory, School of Engineering – Bioengineering, National University of Entre Ríos (UNER). Ruta 11, Km. 10 (3101) Oro Verde, Entre Ríos, Argentina.

Abstract

In previous works we designed and developed a software tool for the optimization of multidimensional-image processing, which consisted of an automatic restoration deconvolution method (positive constrained deconvolution) and three image-restoration indicators (Full-Width at Half-Maximum, Contrast-to-Noise Ratio and Signal-to-Noise Ratio) used to assess the quality of restoration qualitatively. Since the algorithm's design was implemented in uncoupled modules, we were able to introduce two new image-restoration parameters (two three-dimensional Tenegrad-based indicators) without mayor modifications to the script. The enhanced version of the algorithm was used to process raw three-dimensional images using several experimental Point Spread Functions; raw images were obtained by fluorescence wide-field microscopy of epidermal E-cadherin expression in *Rhinella arenarum* embryos and fluorescent microspheres. The image-restoration indicators and the performance of the previous and enhanced versions of the algorithm were compared. Results show that Tenengrad-based indicators concur with the previously used ones and that the new modules do not increase processing time significantly.

Keywords: Automatic algorithm, deconvolution, quantification, microscopy, multidimensional images.

Resumen

En trabajos previos hemos diseñado y desarrollado un software para la optimización del procesamiento de imágenes multidimensionales, el cual consiste de un algoritmo automático de desconvolución de restauración (desconvolución con restricción de positividad) y tres indicadores de restauración de la imágenes (Ancho Total a la Mitad del Máximo, Relación Contraste-Ruido y Relación Señal-Ruido) usados para evaluar cuantitativamente la calidad de restauración. Dado que el diseño del algoritmo se implementó en módulos desacoplados, hemos podido incorporar dos nuevos parámetros para evaluar la restauración de imágenes (indicadores tridimensionales basados en la función de Tenegrad) sin realizar cambios significativos en el código. La versión mejorada del algoritmo se utilizó para procesar imágenes tridimensionales utilizando diversas Funciones de Esparcimiento Puntual experimentales; las imágenes se obtuvieron mediante microscopia de campo amplio de fluorescencia del patrón de expresión de E-caderina en la piel de embriones de *Rhinella arenarum* y de microesferas fluorescentes. Se compararon los indicadores de restauración y el rendimiento de las versiones previa y mejorada del algoritmo. Los resultados indican que los indicadores basados en la función de Tenegrad coinciden con los evaluados previamente y que los nuevos módulos no incrementan significativamente el tiempo de procesamiento.

Palabras claves: Algoritmo automático, desconvolución, cuantificación, microscopia, imágenes multidimensionales

1 INTRODUCTION

The microscope's image formation process is modeled by (1), where (x,y,z) are spatial coordinates, $i(x,y,z)$ is the raw image which is formed by the three-dimensional (3D) convolution (denoted by $\otimes$) of the original object $o(x,y,z)$ and the system's transfer function, denominated Point Spread Function, $PSF(x,y,z)$ [1].

$$i(x, y, z) = o(x, y, z) \otimes PSF(x, y, z) \quad (1)$$

In digital deconvolution microscopy, raw multidimensional images are deconvolved to produce images which resemble the original object more closely [2]. Briefly, this procedure attempts to reverse the modifications brought about by the PSF and in order to accomplish this task a theoretical or experimental PSF is required.

The positive constrained iterative deconvolution method is a restoration algorithm [3] which works in the following manner. First, an estimation of the original object is proposed. Then, the estimate is convolved with an adequate PSF and the resulting image is compared to the raw one, producing correction factors which are used to improve the estimation while ensuring it contains only non-negative values. This process continues until certain exit criteria are met.

Several variables may be evaluated in order to assess the quality of restoration after deconvolution [4][5]. These may be general (such as Contrast-to-Noise Ratio, CNR, Signal-to-Noise Ratio, SNR, and Tenengrad-based indicators) or for a specific specimen (for instance, the Full-Width at Half-Maximum parameter, FWHM, for spherical objects) [6]. CNR and SNR values are calculated using (2) and (3), respectively.

$$CNR = 20\log\left(\frac{Dynamic\ range\ of\ the\ signal}{Standard\ deviation\ of\ the\ noise}\right) \quad (2)$$

$$SNR = 20\log\left(\frac{Mean\ intensity\ of\ the\ signal}{Standard\ deviation\ of\ the\ noise}\right) \quad (3)$$

The Tenengrad function shown in (4) provides a value that indicates the degree of focusing of a given 2D image [7][8], where Ix and Iy are gradient images which result from the convolution of the original image with the Sobel operators [1]. In order to work with 3D images, we propose two 3D Tenengrad-based indicators which are shown in (5) and (6).

$$Tenengrad = \sum_{i=1}^{X}\sum_{j=1}^{Y}\left(I_x^2(i,j) + I_y^2(i,j)\right) \quad (4)$$

$$TEN = \max_{z}\left[\sum_{i=1}^{X}\sum_{j=1}^{Y}\left(I_x^2(i,j) + I_y^2(i,j)\right)\right] \quad (5)$$

$$TENr = \max_z \left[\sum_{i=1}^{X} \sum_{j=1}^{Y} \sqrt{I_x^2(i,j) + I_y^2(i,j)} \right] \quad (6)$$

Since deconvolution enhances high-frequency areas at the expense of low-frequency zones (process modulated by the PSF), deconvolved images have more contrast than their corresponding raw ones, and therefore have higher CNR values. Moreover, deconvolution assigns out-of-focus fluorescence to its correct spatial position; this procedure reduces noise (resulting in higher SNR values) and increases the degree of focus (evidenced by higher TEN and TENr values).

As an example, figure 1 shows CNR, SNR, TEN and TENr values of a raw 2D image (1b) which was sharpened with an unsharp contrast enhancement filter (process equivalent to deconvolution; 1a) and smoothened with a Gaussian low pass filter (procedure comparable to a convolution with a PSF; 1c).

CNR = 35.49   CNR = 15.38   CNR = 9.54
SNR = 51.09   SNR = 30.88   SNR = 25.19
TEN = 9.47_x10^8 TEN = 3.37_x10^8 TEN = 2.04_x10^8
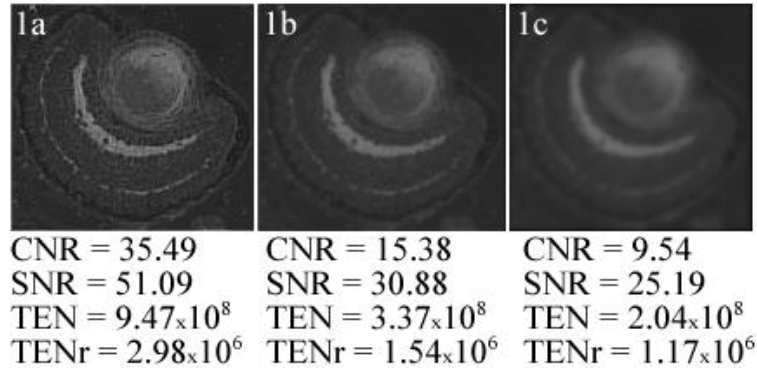TENr = 2.98_x10^6 TENr = 1.54_x10^6 TENr = 1.17_x10^6

Figure 1: CNR, SNR, TEN and TENr values of the raw image after an unsharp contrast enhancement filter was applied (1a), the original raw image (1b) and the raw image after it was smoothened with a Gaussian low pass filter (1c). Images show the total NCAM expression pattern in retinal tissue of *Rhinella arenarum* tapdoles.

The FWHM parameter can be used to measure the diameter of spherical objects such as microspheres. Steps involved in the calculation of the FWHM are as follows. First, an intensity profile is obtained from a path traced through the object's center point. Then, the maximum intensity value *I* is determined and the distance between the two points that correspond to an intensity equal to *I*/2 is provided as the FWHM; this value corresponds to the object's diameter.

In the present work an existing processing algorithm which automatically deconvolved raw images and evaluated image sets after deconvolution was enhanced. Two new image-restoration indicators were added in the form of uncoupled modules to an existing structure which included a restoration deconvolution algorithm (positive constrained iterative method) and three quantification methods (CNR, SNR and FWHM). Given that FWHM, CNR and SNR indicators have been previously implemented and assessed [9], TEN and TENr parameters will be evaluated in the present work; moreover, the performance of both versions of the algorithm will be compared. The improved algorithm was implemented in calculus software (MATLAB v7.0) and was used to process each of four different raw 3D images with thirty PSFs obtained under diverse experimental conditions (five samples of each condition were selected for statistical purposes).

2 MATERIALS AND METHODS

2.1 Hardware and Software

The processing algorithm was implemented in calculus software in a personal computer (Intel Pentium IV 1.81 GHz with 1 GB of RAM and 230 GB of hard-disc space). Raw images were obtained by optical-sectioning [10] using an Olympus BX50 upright microscope, equipped with a white-light source for transmitted microscopy and a mercury UV-lamp for epi-fluorescence microscopy. Images were taken with a cooled monochromatic Apogee CCD camera of 14 bits of resolution, 768x512 pixel^2 sensor size, 9x9 μm^2 pixel size, mounted to the microscope by a mount C lens (0.5X). A stepping motor (RS 440-436) attached to the fine adjustment knob of the microscope enabled the displacement of the stage up and down in steps of multiples of 5 nm [11]; it was controlled via parallel port by a personal computer with an Intel Pentium II 350 MHz processor, 256 MB of RAM and 6 GB of hard-disc space. Images were transferred through Ethernet to the computer in which the processing algorithm was executed.

The CCD camera and stepping motor were controlled by special software which also included deconvolution algorithms [12] and a 3D visualization interface; it was designed in Object Pascal language [13]. Optical sectioning was automatically done by this tool after loading some basic parameters which included image dimensions, time of exposure, distance between in-focus planes and motor speed (which determined stage speed). Images were saved in TIFF 8 bit format and stacks were visualized with the aid of an algorithm which enabled Maximum Intensity Projection (MIP), implemented in OpenGL.

2.1.1 Optical Sectioning

The work-area was selected using a low magnification lens and white light (transmitted) which does not excite the fluorophore and therefore prevents photobleaching [14][15][16]. When switching to UV illumination, the micrometric screw was adjusted to focus using either a 40X (NA 0.85, determining voxels of 0.45x0.45x0.5 μm^3) or 100X objective lens (NA 1.35, 0.18x0.18x0.25 μm^3 voxel size). Then, the stage was moved upwards a distance equal to half the total depth of the future stack and the stepping motor was programmed to move it downwards in step of 0.5 or 0.25 μm (for 40X and 100X, respectively). The final stack size ranged between 128x128x64 and 256x256x256 pixels^3.

2.2 Positive Constrained Deconvolution Method

Figure 2 shows a flowchart of the deconvolution algorithm's sequence. After variable initialization, a normalized PSF is selected and an estimation of the original object is proposed (in this case, the normalized raw image was employed). Then, the Fast Fourier Transform (FFT) is applied to both volumes (transforming them into Fourier space) and their moduli are multiplied pixel-wise (procedure equivalent to a convolution in Real space). The resulting volume is anti-transformed by the inverse FFT (iFFT) and after being compared to the raw image, a new estimation is produced. A non-negativity constraint is imposed on the new estimate since the signal's dynamic range is made up of non-negative values only. This process continues until certain exit criteria are met; in this case, such criteria consisted of a convergence criterion (which was met when the maximum difference e between the estimation and the raw image was no longer significant, that is to say, $e < 1/255$) and a maximum-iteration limitation (establishing that deconvolution cycles would not
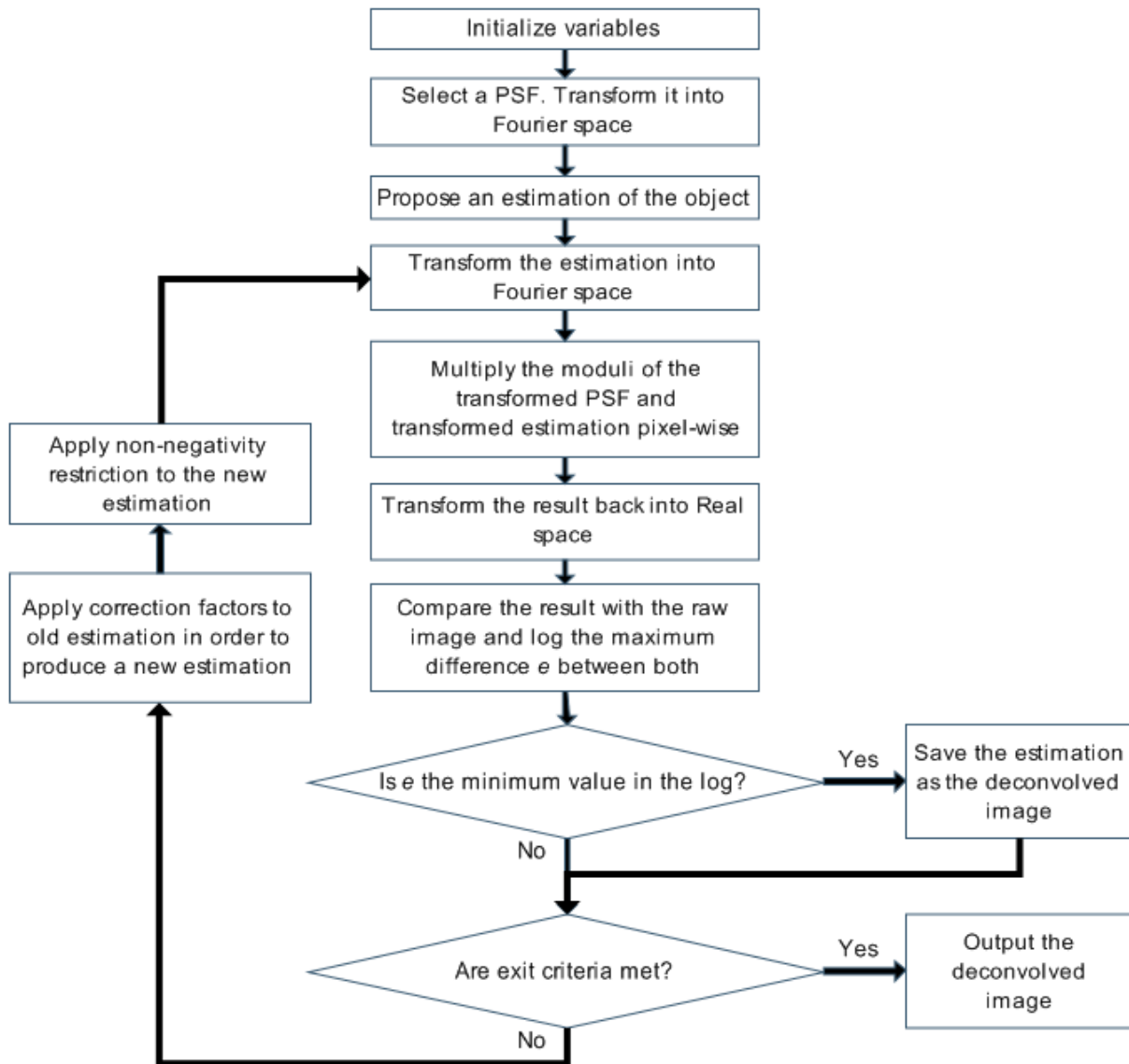
surpass ten iterations).

Figure 2: Steps involved in the positive constrained deconvolution algorithm.

2.3 Quantification Methods

Two general image-quality indicators (TEN and TENr) and a specimen-specific parameter (FWHM) were used to assess the quality of restoration after deconvolution. TEN and TENr were used to evaluate images of epidermal E-cadherin expression in *Rhinella arenarum* embryos, while the FWHM parameter was employed to calculate the diameter of fluorescent microspheres along the x, y and z axis [9].

2.4 PSF Preparation

Fluorescent microspheres (F-8888 kit; Molecular Probes, OR, USA) were used as point-sources of light to produce PSFs under thirty different experimental conditions (five samples of each condition

were selected for statistical purposes). These microspheres were selected according to size so that the Nyquist criterion was satisfied [17]. Consequently, fluorescent beads which were 0.18 and 0.46 μm in diameter were selected for the 40X objective lens, while 0.11-μm and 0.18-μm microspheres were used for the 100X objective lens.

Original solutions containing 0.11-μm, 0.18-μm and 0.46-μm fluorescent microspheres were diluted in distilled water (1:100) and a 5 μL drop of each was placed on a coverslip and left aside until dehydration. Then, these coverslips were placer over slides containing a drop of mounting media. When using the 100X lens, a drop of immersion medium was placed on top of the coverslip. Table 1 summarizes the thirty experimental conditions which were evaluated.

2.5 Specimen Preparation

Two types of specimens were imaged: 4-μm fluorescent microspheres and *Rhinella arenarum* whole embryos incubated with IgG-FITC-anti-E-cadherin. One samples of each specimen was used per objective lens and per PSF-microsphere size, totaling eight 3D raw images.

2.5.1 Fluorescent Microspheres

4-μm fluorescent microspheres were prepared according to the PSF-preparation protocol explained in the previous section, using the ideal condition (see Table 1).

Table 1: Experimental conditions under which PSFs were obtained; ideal conditions are marked with an asterisk (*) [9].

Parameter	40X	100X
Coverslip type (thickness in μm)	0 (80-120) 1 (130-160) 1.5 (160-190) * 2 (190-220)	
Correction-collar value	0.11	-
	0.14	-
	0.17 *	-
	0.20	-
	0.23	-
Mounting medium (refractive index)	Air (1) Water (1.33) Vectashield (1.46) Glycerol [1] (1.47) Oil [2] (1.51) *	
Numerical aperture	-	0.5
	-	1.0
	-	1.35 *
Immersion medium (refractive index)	-	Air (1)
	-	Water (1.33)
	-	Glycerol [1] (1.47)
	-	Oil [2] (1.51) *

[1] Glycerol: Cicarelli, San Lorenzo, Santa Fe, Argentina.
[2] Oil: Olympus, America Inc., Buenos Aires, Argentina.

2.5.2 Rhinella arenarum Embryos

Stage-19 (Gosner, 1960 [18]) *Rhinella arenarum* embryos were treated to study the skin cell-adhesion-molecule E-cadherin [19][20] expression pattern following Larrea's protocols [21][22]. They were fixed in Carnoy, washed in 1X PBS at room temperature and then treated with Triton X-100 (SIGMA Chemical Company, St. Louis, USA) 0.1% in PBS during 30 minutes at room temperature. They were then incubated in goat normal serum 1:20 for 35 minutes followed by anti-E-cadherin antibody (mouse monoclonal antibody; Transduction Laboratories, Lexintong USA) 1:50 at 37°C for 75 minutes. Next, embryos were washed in 1X PBS and incubated with the IgG-FITC (SIGMA) 1:64 at room temperature for 105 minutes and then washed again with 1X PBS; finally, they were mounted in Vectashield mounting medium (Vector Laboratories, Vector Burlingame, CA) to prevent fluorescent decay.

3 RESULTS

Raw images of fluorescent microspheres exhibit an elongated diameter along the z axis which is reduced by deconvolution (Fig. 3). Figure 4 shows this phenomenon for fluorescent microspheres imaged with the 40X objective lenses, which were deconvolved with PSFs obtained using diverse mounting media (Table 1). This bar graph evidences that z-elongation reduction depends on the PSF employed in the deconvolution process. Moreover, it shows that the closer a PSF is to the ideal transfer function, the greater the reduction.
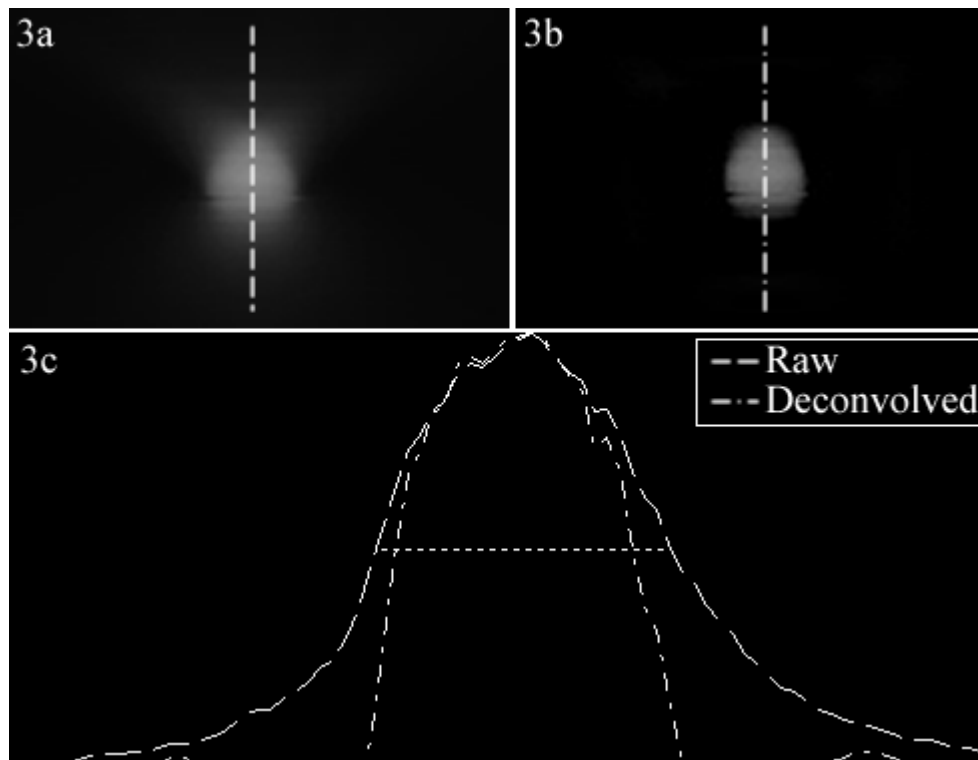

Figure 3: Images show *xz* projections of a raw 4-μm fluorescent microsphere (3a) and the same microsphere after deconvolution with an ideal PSF (3b). Intensity profiles (3c) were traced along paths parallel to the z axis. The dotted line indicates where the FWHM is measured for both curves.

As expected, the values of all image-restoration indicators (CNR, SNR, TEN and TENr) are higher for deconvolved images than for the corresponding raw ones (Fig. 5 and 6). Furthermore, these

values increase as PSF conditions approach ideal ones. TEN and TENr bar graphs (Fig. 6) present greater differences between the diverse experimental conditions than CNR and SNR graphs (Fig. 5) for the same *Rhinella arenarum* skin images.
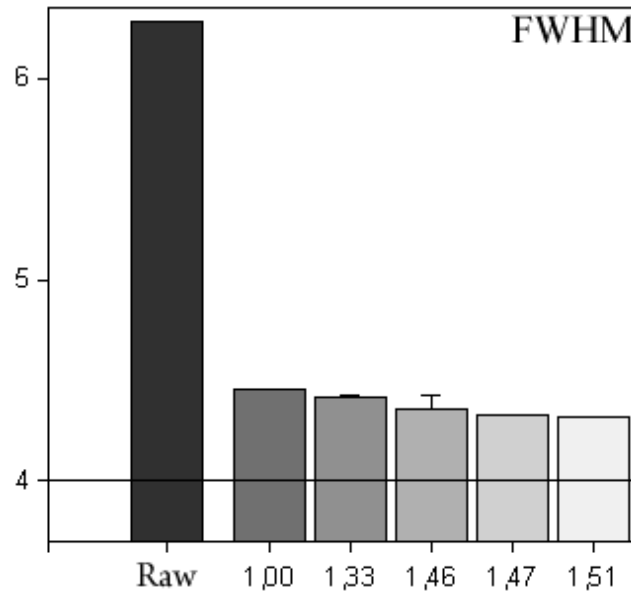

Figure 4: FWHM values for fluorescent microspheres imaged with the 40X objective lens, which were deconvolved with PSFs obtained using 0.46-μm fluorescent microspheres and different mounting media. The horizontal line represents the real microsphere diameter (4 μm).
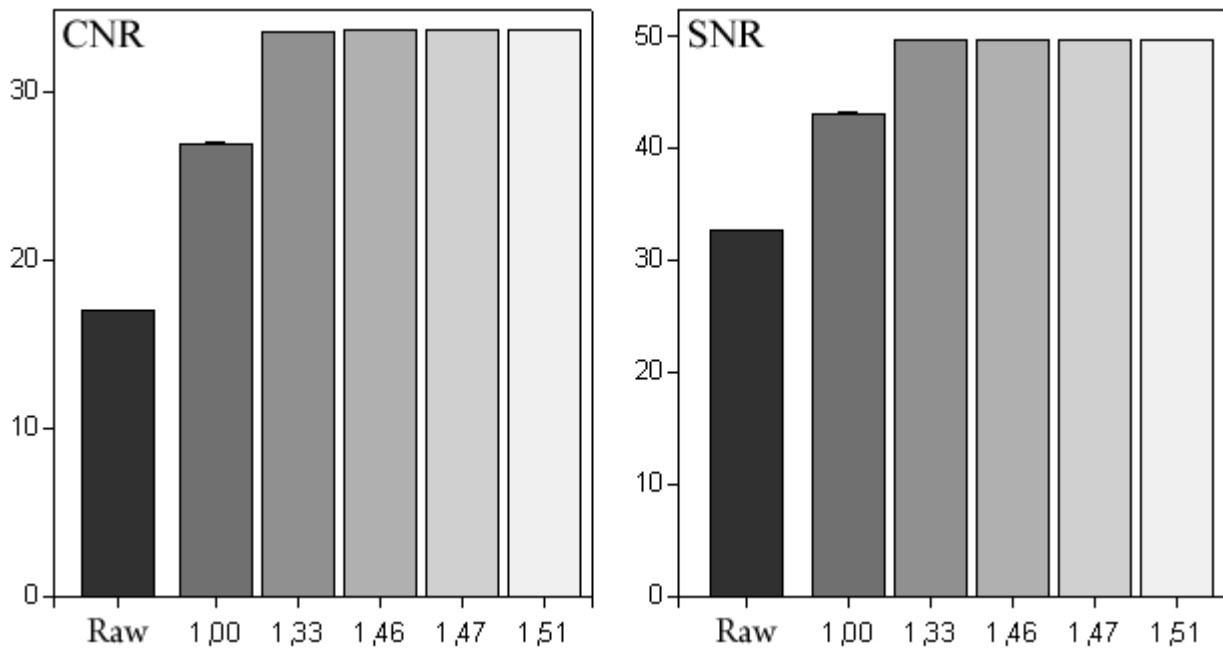

Figure 5: CNR and SNR values for epidermal E-cadherin expression in *Rhinella arenarum* embryos imaged with the 40X objective lens, which were deconvolved with PSFs obtained using 0.46-μm fluorescent microspheres and different mounting media.
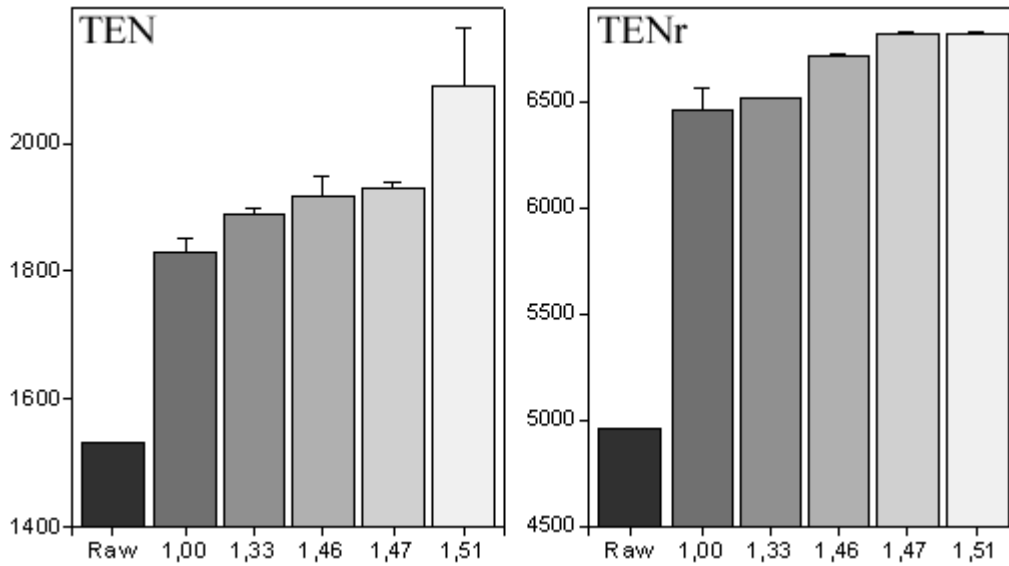
Figure 6: TEN and TENr values for epidermal E-cadherin expression in *Rhinella arenarum* embryos imaged with the 40X objective lens, which were deconvolved with PSFs obtained using 0.46-µm fluorescent microspheres and different mounting media.

Time is an important factor that must be taken into consideration when working with large volumes of information. A comparison table showing the time taken to process all raw images with the previous and enhanced versions of the processing algorithm is shown in Table 2.

Table 2: Time taken to apply the previous and enhanced versions of the processing algorithm to all raw images.

Specimen	Image size	Processing time	
		Previous version	Enhanced version
Fluorescent microsphere	256x256x64 pixels^3	73 minutes	73 minutes
	128x128x64 pixels^3	64 minutes	64 minutes
Epidermal E-cadherin expression pattern (*Rhinella arenarum* embryo)	128x128x128 pixels^3	127 minutes	121 minutes
	128x128x256 pixels^3	138 minutes	141 minutes

3 DISCUSSION AND CONCLUSIONS

In the present work, an existing processing algorithm for digital deconvolution microscopy was enhanced by the addition of two new image-restoration indicators (TEN and TENr). Results obtained with these indicators are concordant with previously obtained results using CNR, SNR and FWHM parameters [9]. These have demonstrated that deconvolution is sensitive to variations in the PSF and that the best restoration results are achieved when PSFs obtained under conditions similar to ideal ones are employed (Fig. 4 through 6).

Both versions of the automatic algorithm convey a significant reduction in processing time (Table

2). It took under seven hours to complete the image processing task, that is to say, to deconvolve each of four raw 3D images with a hundred and fifty different PSFs (thirty experimental conditions, n = 5), that is to say 600 different deconvolutions, followed by the evaluation of the resulting deconvolved images with at least one of five image-restoration quantification methods. If the same task was carried out manually, it would take an operator days or weeks. Furthermore, the processing time of both versions of the algorithm differ in less than 5 %; we can therefore conclude that the new modules do not reduce the algorithm's performance.

In order to perform an accurate quantification, a restoration deconvolution method was selected since deblurring tools eliminate potentially-useful information. Other deconvolution and quantification methods may be added or may replace the present ones with minor adjustments to the code due to the uncoupled-module design of the processing algorithm. Methods contained in new modules should ensure that data is not lost during processing because an incorrect treatment of the samples will lead to inappropriate quantitative analyses. Additionally, the algorithm is an unbiased method of evaluation which eliminates non-systematic errors in the quantification process since it is independent of the operator.

The present algorithm is readily applied to multidimensional images produced by other techniques such as transmitted-light and confocal microscopy. Furthermore, other image formats (such as JPEG, BMP, GIF and PNG) are currently supported in addition to the TIFF files employed in the present work.

In future works we plan to continue improving the present algorithm by the addition of new modules. We plan to implement other quantification methods to assess image restoration after deconvolution, such as sharpness indicators which may include the normalized variation parameters. Additionally, new deconvolution methods might be added to the algorithm (for instance, a blind deconvolution method). Moreover, a new version of the mentioned algorithm may be programmed using an object-based language (such as C++) so as to provide microscopy users with a standalone software with a user-friendly interface.

REFERENCES

[1] Castleman K.R. *Digital Image Processing*. Prentice Hall, New Jersey, 1996.

[2] Sarder P. and Nehorai A. Deconvolution methods for 3-D fluorescence microscopy images. *IEEE Signal Processing Magazine*, 23:32-45, May 2006.

[3] Wallace W., Schaefer L.H. and Swedlow J.R. A workingperson's guide to deconvolution in light microscopy. *Biotechniques*, 31:1076-1097, 2001.

[4] Grgic S., Grgic M. and Mrak M. Reliability of objective picture quality measures. *Journal of Electrical Engineering*, 55:3-10, 2004.

[5] Yao Y., Abidi B.R. and Abidi M.A. Extreme Zoom Surveillance: System Design and Image Restoration. *Journal of Multimedia*, 2:20-31, 2007.

[6] Adur J.F. Determinación de las propiedades ópticas de un sistema de epifluorescencia y su utilización en estudios de microscopía cuantitativa de 3D. *Biomedical Engineer Magister Thesis*, Faculty of Engineering – Bioengineering. Entre Ríos National University. Argentina. 2006.

[7] Conchello J.A. and Lichtman J.W. Optical sectioning microscopy. *Nature Methods*, 2:920-931, 2005.

[8] Santos A., Ortiz de Solórzano C., Vaquero J.J., Peña J.M., Mapica N. and Del Pozo F. Evaluation of autofocus functions in molecular cytogenetic analysis. *Journal of Microscopy*, 188:264-272, 1997.

[9] Vicente N.B., Diaz Zamboni J.E., Adur J.F., Izaguirre M.F. and Casco V.H. Design and validation of an automatic algorithm for deconvolution and quantification in modern microscopy. In *Argentine Symposium on Computing Technology (AST)*, 2008.

[10] Krotkov E. Focusing. *International Journal of Computer Vision*. 1:223-237, 1987.

[11] Adur J. and Schlegel J. Design, development and construction of an advance micrometric system for microscopes. *Bioengineering Degree Thesis*, Faculty of Engineering – Bioengineering. Entre Ríos National University. Argentina. 1997.

[12] Diaz-Zamboni J.E., Adur J.F., Fiorucci M.P., Izaguirre F. and Casco V.H. Algoritmo de desconvolución iterativo con restricción de positividad para imágenes de microscopía de fluorescencia tridimensional. In *XV Congreso Argentino de Bioingeniería*, 2005.

[13] Diaz-Zamboni J.E. Software para usuarios de microscopía de desconvolución digital. *Bioengineering Degree Thesis*, Faculty of Engineering – Bioengineering, Entre Ríos National University, Argentina, 2004.

[14] Vicente N.B., Diaz Zamboni J.E., Adur J.F., Paravani E.V. and Casco V.H. Photobleaching correction in fluorescence microscopy images. *Journal of Physics: Conference Series*, doi: 10.1088/1742-6596/90/1/012068, 2007.

[15] Benson D.M., Bryan J., Plant A.L., Gotto A.M. and Smith L.C. Digital imaging fluorescence microscopy: spatial heterogeneity of photobleaching rate constants in individual cells. *The Journal of Cell Biology*, 100:1309-1323, 1985.

[16] Song L., Hennink E.J., Young T. and Tanke H.J. Photobleaching kinetics of fluorescein in quantitative fluorescence microscopy. *Biophysical Journal*, 68:2588-2600, 1995.

[17] Sibarita J.B. Deconvolution microscopy. *Advances in Biochemical Engineering/Biotechnology*, 95: 201–243, 2005.

[18] Gosner K.L. A simplified table for stanging anuran embryos and larval with noter on identification. *Herpetologica*, 16:183-190, 1960.

[19] Adams C.L., Chen Y.T., Smith S.J. and Nelson W.J. Mechanisms of epithelial cell–cell adhesion and cell compaction revealed by high-resolution tracking of E-Cadherin–Green Fluorescent Protein. *The Journal of Cell Biology*, 142:1105-1119, 1998.

[20] Gumbiner B.M. Cell adhesion: the molecular basis of tissue architecture and morphogenesis. *Cell*, 84:345-357, 1996.

[21] Izaguirre M.F., Adur J.F., Peralta-Soler A. and Casco V.H. Alterations induced by E-Cadherin and β-catenin antibodies during the development of Bufo arenarum (Anura – Bufonidae). *Histology and Histopathology*, 16:1097-1106, 2001.

[22] Larrea D., Díaz-Zamboni J.E., Adur J.F., Izaguirre M.F. and Casco V.H. Expresión tridimensional de cadherina E, alfa- y beta-catenina en la piel, durante el desarrollo de Bufo arenarum. In *IX Jornadas de Ciencias Naturales del Litoral y Reunión Argentina de Ciencias Naturales*. Paraná, Argentina. 2006.